8.A.8 Nuclear Physics B9 (1969) 331-348. North-Holland Publ. Comp., Amsterdam

LONGITUDINAL PHASE-SPACE PLOTS OF MULTIPARTICLE HADRON COLLISIONS AT HIGH ENERGY

L. VAN HOVE
CERN - Geneva

Received 9 January 1969

Abstract: The accurate study of collisions with more than two particles in the final state is greatly hampered by the high dimensionality of the phase space in which the distribution of final states must be investigated. Taking advantage of the fact that in hadron collisions at high energy all transverse momenta remain generally small, we separate phase space into its longitudinal and transverse parts, and we show that for a n-particle collision the longitudinal phase-space distribution reduces to a manifold of dimension $n-2$. We study the main properties of longitudinal phase-space plots, the way in which relativistically invariant subenergies and momentum transfers vary along them, as well as the qualitative properties of reggeized multiperipheral amplitudes. The longitudinal phase-space plot is parametrized by new angular variables $\omega_1, \ldots \omega_{n-2}$ and the interest of plotting events against them is demonstrated. The paper ends with a new method for Monte Carlo integration of phase-space integrals.

1. INTRODUCTION

The dynamical study of hadron collisions with more than two particles in the final state is greatly hampered by the high dimensionality of phase space. The common procedures of plotting single particle momentum distributions or two-particle effective mass distributions give only a very incomplete reflection of the true experimental phase-space distribution, and they are therefore of limited use for discovering empirical characteristics of the data as well as for testing experimentally the dynamical models proposed by strong interaction theory.

As suggested earlier [1], we believe that these difficulties can be alleviated in the case of multiparticle collisions at high energy (incident lab energy $E_{\text{lab}} > 8$ GeV) by means of longitudinal phase-space plots. The usefulness of these plots stems from the well-known empirical fact that the transverse momenta of outgoing particles are restricted to small values, their average being of order 0.3 to 0.4 GeV/c for pions and protons respectively, and are largely independent of incident energy. Concequently, when the latter is large, the phase-space distribution extends mainly in the directions corresponding to large longitudinal momenta, and many of its

characteristic features can already be read from analyzing its projection on longitudinal phase space.

The present paper describes the main kinematic properties of longitudinal phase-space plots, especially for 3 and 4 particle collisions, in the approximation where the masses and the transverse momenta are small compared with the incident center-of-mass (c.m.) momentum (sects. 2 and 3). It discusses the distribution of invariant subenergies and momentum transfers in longitudinal phase space, as well as the qualitative properties of double Regge amplitudes for a three-particle collision (sects. 4 and 5). It also proposes a new method for Monte Carlo integration of (complete) phase-space integrals which should become useful when the above approximation holds (sect. 6 and appendix).

2. LONGITUDINAL PHASE SPACE AT HIGH ENERGY AND SMALL TRANSVERSE MOMENTA

We consider the collision $A+B \rightarrow C_1 + \ldots C_n$. Let W be its total c.m. energy. We denote the c.m. longitudinal momentum of C_i by q_i, its transverse momentum by $\boldsymbol{r}_i$ and its c.m. energy by

$$E_i = (m_i^2 + \boldsymbol{r}_i^2 + q_i^2)^{\frac{1}{2}} = (m_i'^2 + q_i^2)^{\frac{1}{2}} , \tag{1}$$

$$m_i' = (m_i^2 + \boldsymbol{r}_i^2)^{\frac{1}{2}} . \tag{2}$$

Here, m_i' can be called an effective mass for longitudinal motion. We have of course

$$\sum_1^n E_i = W , \qquad \sum_1^n q_i = 0 , \qquad \sum_1^n \boldsymbol{r}_i = 0 . \tag{3}$$

We propose to represent each individual collision by the point of coordinates $q_1, \ldots q_n$ in the n-dimensional euclidean space S_n. Momentum conservation, eq. (3), implies that all such points lie in the $(n-1)$- dimensional hyperplane L_{n-1} of equation $\sum q_i = 0$. We call L_{n-1} the *longitudinal phase space*. For fixed values of the $\boldsymbol{r}_i$ and hence of the m_i', the points $(q_1, \ldots q_n)$ lie on the $(n-2)$- dimensional hypersurface K_{n-2} defined in L_{n-1} by the equation

$$\sum_1^n (m_i'^2 + q_i^2)^{\frac{1}{2}} = W . \tag{4}$$

When all $q_i^2 \gg m_i'^2$, this equation reduces to

$$\sum_1^n |q_i| = W , \tag{5}$$

which defines a polyhedron H_{n-2} in L_{n-1}. Its plane faces obtain for all $q_i \neq 0$. Its 'sides' of dimensionalities n-3, n-4, ..., and its vertices correspond to points $(q_1, \ldots q_n)$ where 1, 2, ..., n-3, and n-2 of the q_i vanish. For these q_i, the approximation of neglecting m'_i is not valid, and it is therefore along the sides and vertices that K_{n-2} deviates most strongly from H_{n-2}. In particular for $q_i^2 \ll m_i'^2$, one has

$$(m_i'^2 + q_i^2)^{\frac{1}{2}} \approx m'_i + (q_i^2/2m'_i) \ . \tag{6}$$

This formula shows that the shape of the hypersurface K_{n-2} differs from the polyhedron H_{n-2} mainly through the fact the latter's sides and vertices are rounded off. This rounding off depends on the m'_i, i.e. on the masses m_i and the transverse momenta $\boldsymbol{r}_i$. As shown by eq. (6), the rounding off corresponds to a distance of order m'_i between K_{n-2} and H_{n-2} along the side where $q_i = 0$. This is small compared to the overall size of H_{n-2} and K_{n-2}, which is of order W. The hypersurface K_{n-2} is always inside H_{n-2}, and K_{n-2} for non-vanishing $\boldsymbol{r}_i$ is always inside K_{n-2} for all $\boldsymbol{r}_i = 0$.

Fig. 1 shows, for a three-body collision (n=3), the plane L_2 containing the polyhedron H_1, which is a regular hexagon, as well as the manifold K_1, here a curve, for two sets of transverse momenta. The parameters are

$$W = 4 \ , \qquad m_1 = m_2 = m_\pi \ , \qquad m_3 = m_N \ ,$$

($m_\pi = 0.14$ = pion mass, $m_N = 0.94$ = nucleon mass)

$$\boldsymbol{r}_1 = \boldsymbol{r}_2 = \boldsymbol{r}_3 = 0 \ , \qquad \text{(outer curve } K_1) \ ,$$

$$|\boldsymbol{r}_1| = |\boldsymbol{r}_2| = 0.4 \ , \qquad |\boldsymbol{r}_3| = 0.5 \ , \qquad \text{(inner curve } K_1) \ .$$

Here and below all quantities are in GeV, with the convention $c = 1$. In terms of polar coordinates q, ω in the plane L_2, the q_i belonging to its points are found to be

$$q_1 = \sqrt{\tfrac{2}{3}}\ q \sin\omega \ , \qquad q_2 = \sqrt{\tfrac{2}{3}}\ q[-\tfrac{1}{2}\sin\omega - \tfrac{1}{2}\sqrt{3}\cos\omega] \ ,$$

$$q_3 = \sqrt{\tfrac{2}{3}}\ q[-\tfrac{1}{2}\sin\omega + \tfrac{1}{2}\sqrt{3}\cos\omega] \ , \tag{7}$$

with $q = (q_1^2 + q_2^2 + q_3^2)^{\frac{1}{2}}$. The q_i are $\sqrt{\frac{2}{3}}$ times the distances of its points to the lines $q_i = 0$. The scale shown in fig. 1 has been readjusted by this factor $\sqrt{\frac{2}{3}}$, so that in this scale the q_i are the distances themselves to the lines $q_i = 0$, while the distance to the origin 0 is now $\sqrt{\frac{2}{3}}\ q$. The regions of positive and negative q_i are indicated by + and - signs. Fig. 2 shows the hexagon H_1 and the curve K_1 for $W = 16$, the other parameters being the same as for the inner curve of fig. 1.

Fig. 3 presents the experimental distribution of events in the longitudinal phase space L_2 for the reaction $\pi^+ p \to \pi^+\pi^0 p$ at pion lab momentum 8 GeV/c, which closely corresponds to $W = 4$ (ref. [2]). The longitudinal momenta q_i are here denoted by P_L^* and the corresponding particle. The outer curve is K_1 for vanishing transverse momenta of all three particles.

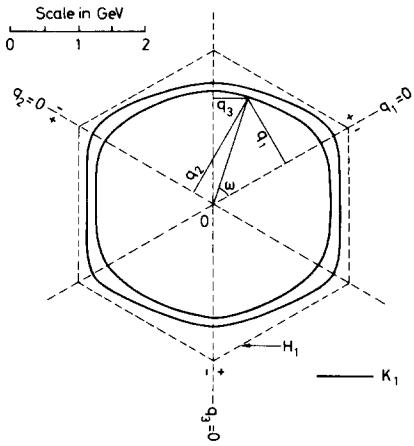

Fig. 1. Longitudinal phase-space plot for $\pi\pi$N at c.m. energy W = 4 GeV. The inner full curve is K_1 for transverse momenta 0.4, 0.4, 0.5 GeV/c respectively, the outer one is K_1 for vanishing transverse momenta. The dashed line represents the hexagon H_1. For the definition of the scale, see the text.

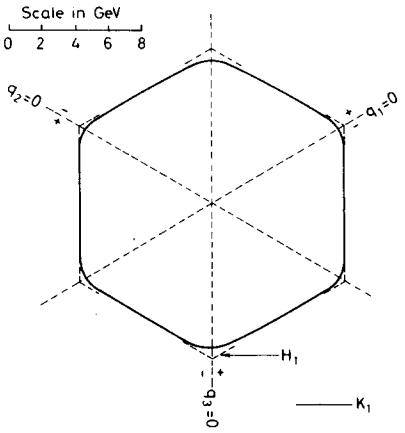

Fig. 2. Longitudinal phase-space plot for $\pi\pi$N at c.m. energy W = 16 GeV. The full curve is K_1 for transverse momenta 0.4, 0.4, 0.5 GeV/c. The dashed lines represent the hexagon H_1 near its vertices. The scale is the same as defined in the text for fig. 1.

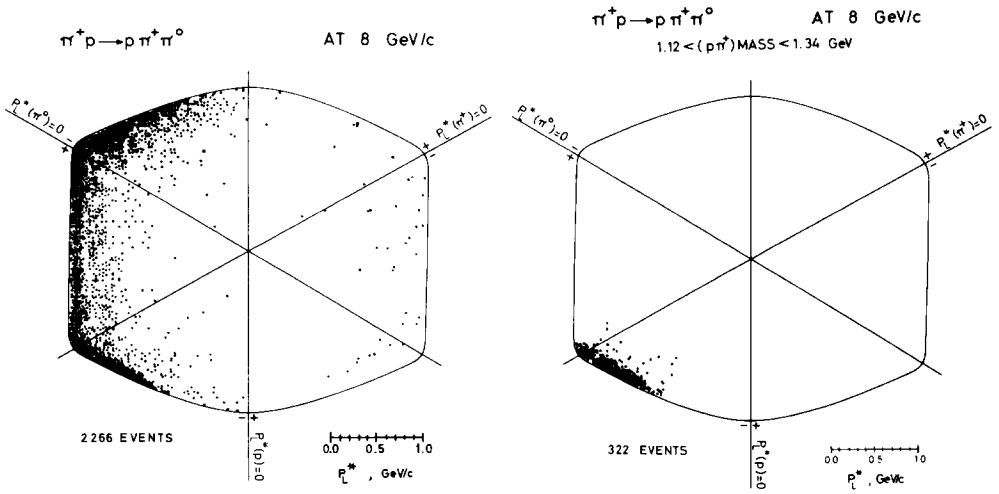

Fig. 3. Experimental longitudinal phase-space plot for $\pi^+p \rightarrow \pi^+\pi^o p$ at lab momentum 8 GeV/c, from Aachen-Berlin-CERN Collaboration [2]. The longitudinal momenta are here denoted by p_L^*. Fig. 3a contains all events, fig. 3b those where π^+p is in the N^{*++} region. The latter figure illustrates the location of a resonance on the plot (see also sect. 4). The curve is K_1 for vanishing transverse momenta. The scale is defined as specified in the text for fig. 1.

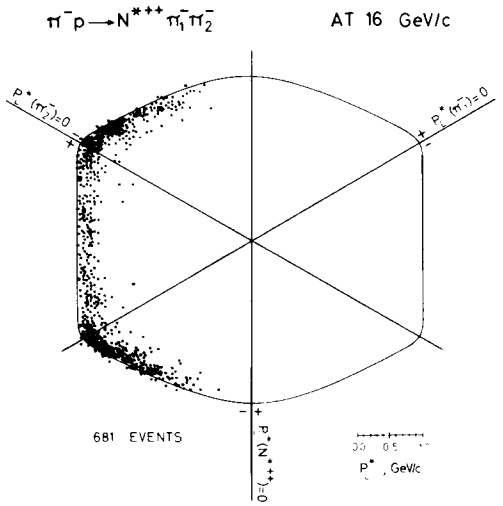

Fig. 4. Experimental longitudinal phase-space plot for $\pi^-p \rightarrow \pi^-\pi^- N^{*++}$ at lab momentum 16 GeV/c, from Aachen-Berlin-Bonn-CERN-Heidelberg Collaboration [3]. All events are included. The curve is K_1 for vanishing transverse momenta, the N^{*++} mass having its central value. The spread of this mass explains that some points fall outside the curve. The scale is defined as specified in the text for fig. 1.

The experimental distribution for $\pi^-p \rightarrow \pi^-\pi^- N^{*++}$ at 16 GeV/c [3] is given in fig. 4.

For four-body collisions (n=4), the longitudinal phase space L_3 has three dimensions. The polyhedron H_2 is shown in fig. 5. In the original metric of the S_4 space of points $(q_1, \ldots q_4)$, the q_i are the distances to the planes OAB, OBD, OCE and OAE respectively, each multiplied by $\frac{1}{2}\sqrt{3}$ (this factor would be $(n-1)^{\frac{1}{2}}/n^{\frac{1}{2}}$ for general n). The sign of the distances is so defined that $q_1 > 0$, $q_{2,3,4} < 0$ for the point P in fig. 5. The square faces of H_2 carry points for which two q_i are positive and two negative, the points on the triangular faces have three q_i of the same sign (and hence the fourth with the opposite sign). All sides of H_2 are equal. The surface K_2, not shown in fig. 5, differs from H_2 mainly by the rounding off of sides and vertices.

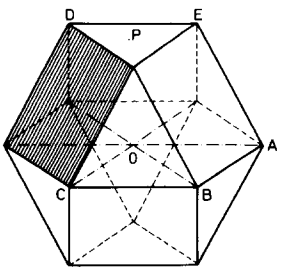

Fig. 5. The polyhedron H_2 in the longitudinal phase space of a four-particle collision (n=4). The hatched face is defined in sect. 4.

3. VOLUME ELEMENT IN LONGITUDINAL PHASE SPACE

We discuss in this section the relativistically invariant volume element in phase space

$$dV_R = \left(\prod_1^n E_i\right)^{-1} dV_N$$

where dV_N, the non-relativistic volume element into the c.m. system, separates into

$$dV_N = dV^T dV_N^L, \quad (T = \text{transverse}, \ L = \text{longitudinal})$$

$$dV^T = \delta_2\left(\sum_1^n \boldsymbol{r}_i\right) \prod_1^n d_2 \boldsymbol{r}_i \ ,$$

$$dV_N^L = \delta\left(\sum_1^n q_i\right) \delta\left(\sum_1^n (m_i'^2 + q_i^2)^{\frac{1}{2}} - W\right) \prod_1^n dq_i \ .$$

We are concerned with the longitudinal element dV_N^L at fixed values of the m_i' (i.e. of the $|\boldsymbol{r}_i|$). In the space S_n we go over to the cylindrical coordinates $\omega_1, \ldots \omega_{n-2}$, q and Q depicted in fig. 6 (for n=3). The $\omega_1, \ldots \omega_{n-2}$ are polar angle coordinates in the hyperplane L_{n-1} (in fig. 6 there is only one angle ω). The lengths q and Q are the distances OP', PP' respectively, where PP' is perpendicular to L_{n-1}. They are given in sign and magnitude by

$$Q = n^{-\frac{1}{2}} \sum_1^n q_i \ , \qquad q = \left[\left(\sum_1^n q_i^2\right) - Q^2\right]^{\frac{1}{2}} \geqslant 0 \ .$$

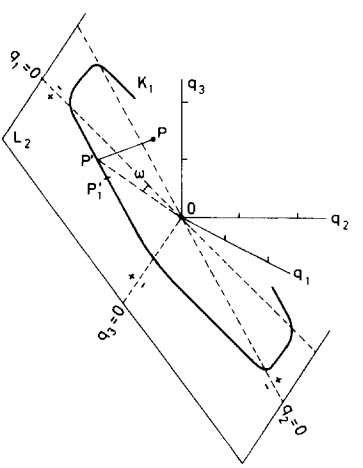

Fig. 6. The longitudinal phase space for a three-particle collision (n=3) and the definition of the variables ω, q = OP' and Q = P'P.

Now dV_N^L is easily transformed into

$$dV_N^L = n^{-\frac{1}{2}}\,\delta(Q)dQ\cdot\delta(q-q_0)dq\cdot D_N d_{n-2}\,\omega\,,$$

where $d_{n-2}\,\omega$ is the element of solid angle $\omega_1,\ldots\omega_{n-2}$ (or equivalently the hypersurface element on the unit hypersphere in L_{n-1}), and q_0, D_N are functions of W, $m_1,\ldots m_n'$ and $\omega_1,\ldots\omega_{n-2}$ defined by

$$\sum_1^n (m_i'^2 + q_0^2\gamma_i^2)^{\frac{1}{2}} = W\,, \qquad q_0 \geqslant 0\,, \tag{8}$$

$$D_N = q^{n-2}\Big/\frac{\partial}{\partial q}\Big[\sum_1^n (m_i'^2 + q^2\gamma_i^2)^{\frac{1}{2}}\Big] \text{ at } q = q_0\,. \tag{9}$$

Here the γ_i are the directional cosines of $(q_1,\ldots q_n)$ in S_n:

$$q_i = (q^2+Q^2)^{\frac{1}{2}}\,\gamma_i\,, \qquad \sum_1^n \gamma_i^2 = 1\,. \tag{10}$$

When the point $(q_1,\ldots q_n)$ is in L_{n-1} (i.e. $Q=0$), the γ_i are functions of $\omega_1,\ldots\omega_{n-2}$ only. For n=3, they are the quantities multiplying q in eq. (7). Note that the root q_0 of eq. (8) exists only when

$$W > \sum_1^n m_i'\,, \tag{11}$$

which is a condition on transverse momenta. The relativistic volume element now is

$$dV_R = dV^T dV_R^L\,,$$

$$dV_R^L = n^{-\frac{1}{2}}\,\delta(Q)dQ\cdot\delta(q-q_0)dq\cdot D_R d_{n-2}\omega\,,$$

$$D_R = \Big[\prod_1^n (m_i'^2 + q_0^2\gamma_i^2)\Big]^{-\frac{1}{2}}\cdot D_N$$

Fig. 7 shows D_N and D_R for n=3 as functions of the angle ω of fig. 6. They are normalized to maximum value one, and the parameters used are

$$W = 4\,, \qquad m_1 = m_2 = m_\pi\,, \qquad m_3 = m_N\,,$$
$$|r_1| = |r_2| = 0.4\,, \qquad |r_3| = 0.5\,. \tag{12}$$

In the approximation where all $q_i \gg m_i'$, eqs. (8) and (9) become

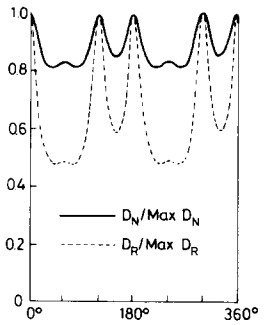

Fig. 7. The non-relativistic and relativistic phase-space weight functions D_N and D_R for n=3 plotted against the angle ω and normalized to maximum value one. The curves refer to $\pi\pi$N at c.m. energy W = 4 GeV and transverse momenta 0.4, 0.4 and 0.5 GeV/c.

$$q_0 \approx W\Big[\sum_1^n |\gamma_i|\Big]^{-1} ,$$

$$D_N \approx W^{-1}\, q_0^{n-1} .$$

It is then easy to verify that, on each face of the polyhedron H_{n-2} to which K_{n-2} reduces in this approximation, one has

$$D_N\, d_{n-2}\omega \approx c\, d_{n-2}\Sigma$$

Here $d_{n-2}\Sigma$ is the hypersurface element on H_{n-2} (for n=3, $d_1\Sigma$ is the line element $P'P'_1$ in fig. 6), and c remains constant on each face, its value being

$$c = \tfrac{1}{2}[n/j(n-j)]^{\frac{1}{2}} ,$$

on a face where j of the variables $q_1, \ldots q_n$ have one sign and n-j the opposite one.

4. INVARIANT SUBENERGIES AND MOMENTUM TRANSFERS

Dynamical studies of multiparticle collisions make much use of relativistically invariant variables, especially the two-particle subenergies

$$s_{ij} = (p_i+p_j)^2 = m_i^2 + m_j^2 + 2E_iE_j - 2q_iq_j - 2\,\boldsymbol{r}_i\cdot\boldsymbol{r}_j ,$$

and the single particle momentum transfers

$$t_i = (p_A - p_i)^2 = m_A^2 + m_i^2 - 2E_AE_i + 2q_Aq_i ,$$

$$t' = (p_B - p_i)^2 = m_B^2 + m_i^2 - 2E_BE_i + 2q_Bq_i .$$

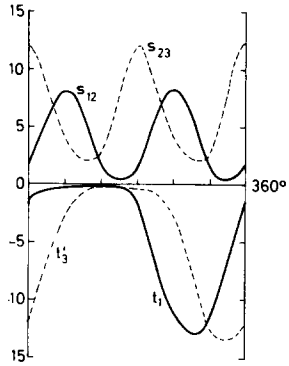

Fig. 8. The subenergies s_{12}, s_{23} and the momentum transfer t_1, t_3' plotted as function of the angle ω for the collision $\pi N \to \pi\pi N$ at c.m. energy 4 GeV and transverse momenta 0.4, 0.4, 0.5 GeV/c for the outgoing particles. The vertical scale is in $(\mathrm{GeV})^2$.

The p denote the four-momenta of the particles and $q_A = -q_B$ the incident (purely longitudinal) c.m. momentum. For n=3 and the parameters (12), the quantities s_{12}, s_{23}, t_1 and t_3' are plotted against the angle ω in fig. 8; the incident particles are taken to be A = π, B = N. Increasing the c.m. energy to W = 16 for the same masses and transverse momenta, we obtain fig. 9. The polygonal shape now taken by the curves is striking. It can be understood as follows. In the limit of large energy one has, for any n and in the notations of sect. 3, the expansion

$$s_{ij} \approx 2W^2[\,|\gamma_i\gamma_j| - \gamma_i\gamma_j]\Big(\sum_1^n |\gamma_k|\Big)^{-2} + m_i^2 + m_j^2 + m_i'^2\,|\gamma_j/\gamma_i| + m_j'^2\,|\gamma_i/\gamma_j| - 2\boldsymbol{r}_i\cdot\boldsymbol{r}_j + \ldots,$$

$$t_i \approx -W^2[\,|\gamma_i| - \gamma_i]\Big(\sum_1^n |\gamma_k|\Big)^{-1} + m_A^2[1 - 2\,|\gamma_i|\Big(\sum_1^n |\gamma_k|\Big)^{-1}] + m_i^2 - m_i'^2\Big(\sum_1^n |\gamma_k|\Big)\,|2\gamma_i|^{-1} + \ldots,$$

$$t_i' \approx -W^2[\,|\gamma_i| + \gamma_i]\Big(\sum_1^n |\gamma_k|\Big)^{-1} + m_B^2[1 - 2\,|\gamma_i|\Big(\sum_1^n |\gamma_k|\Big)^{-1}] + m_i^2 - m_i'^2\Big(\sum_1^n |\gamma_k|\Big)\,|2\gamma_i|^{-1} + \ldots.$$

The terms neglected are of order W^{-2}. The characteristic of these formulae is that their first line gives essentially linear variations over an interval of order W^2 as long as $\gamma_i\gamma_j$, γ_i or $-\gamma_i$ is negative, but vanishes otherwise. The following lines give finite expressions independent of W; their

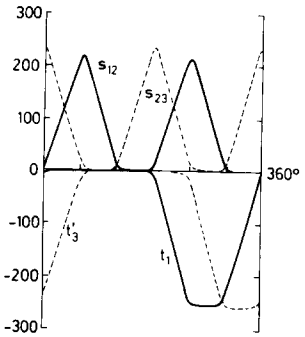

Fig. 9. Same quantities as in fig. 8, except that the c.m. energy is here 16 GeV.

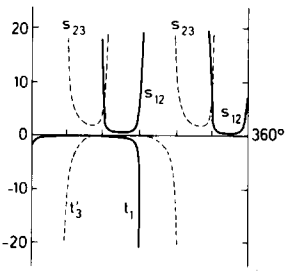

Fig. 10. Enlarged view of the small s and $|t|$ region of fig. 9. The vertical scale is again in $(\mathrm{GeV})^2$.

shape is illustrated for n=3 in fig. 10 which shows the middle section of fig. 9 on an enlarged scale. The regions where s_{ij}, t_i or t'_i remain finite even for large W are easily recognized in kinematic terms:

s_{ij} finite, $\gamma_i\gamma_j$ or $q_iq_j > 0$: the particles C_i and C_j go both forward or both backward in the c.m. system;

t_i finite, $\gamma_i > 0$ or $q_i > 0$: C_i goes forward in the c.m. system;

t'_i finite, $\gamma_i < 0$ or $q_i < 0$: C_i goes backward in the c.m. system.

As clearly seen for n=3 in fig. 10, the region where s_{12} and s_{23} are both large and $|t_1|$, $|t'_3|$ both finite (region of 'double Regge behaviour', see sect. 5) is limited to the immediate neighbourhood of $\omega = 120^\circ$.

The above discussion, and especially the expansions of s_{ij}, t_i, t'_j for large W, show that the sides and vertices of the polyhedron H_{n-2}, i.e. the configurations where one or more q_i vanish, have at high energy a relativistically invariant meaning through the fact that they correspond to sharp breaks in the variations of invariant subenergies and momentum transfers. The discussion also allows to locate the regions of the longitudinal phase-space plot where two or more final particles form a resonance (see fig. 3b for an experimental example).

Another type of invariant momentum transfer which is often considered is defined by

$$t(i_1, \ldots i_j) = (p_A - p_{i_1} \ldots - p_{i_j})^2 = (p_B - p_{i_{j+1}} \ldots - p_{i_n})^2 \ .$$

Its asymptotic behaviour for $W \to \infty$ can be discussed by the type of expansion already used. We restrict ourselves here to the remark that, for $W \to \infty$, the region of $K_{n-2} \approx H_{n-2}$ where $|t(i_1, \ldots i_j)|$ remains finite is the

set of faces of H_{n-2} on which all $q_{i_1}, \ldots q_{i_j} > 0$ and/or all $q_{i_{j+1}}, \ldots q_{i_n} < 0$. For example, for $t(1,2)$ and $n=4$, this region is composed of the hatched square face and the four adjacent triangular faces in fig. 5. The proof of our general statement is the following. Consider $t(1, \ldots j)$ and neglect all masses and transverse momenta. One can then write

$$t(1, \ldots j) = [\,|q_A| + q_A - \sum_1^j (|q_i| + q_i)] \cdot [\,|q_A| - q_A - \sum_1^j (|q_i| - q_i)] \,.$$

A being forward, $|q_A| = q_A$. If all $q_1, \ldots q_j > 0$, the second factor vanishes. If all $q_{j+1}, \ldots q_n < 0$, the forward particles are all among $C_1, \ldots C_j$ and they give the non-vanishing terms in

$$\sum_1^j (|q_i| + q_i) \,.$$

Energy conservation then makes this sum equal to $2\,|q_A|$.

5. MULTIPERIPHERAL REGGE MODEL

Considerable success has been reached by the Regge version of the multiperipheral model in accounting for the observed single particle distributions in multiparticle collisions [4]. Use of longitudinal phase-space plots can be expected to provide many new tests of such models and, more generally, to give more concrete insight into the dynamical behaviour of the collisions. We limit ourselves here to a brief discussion of the model for $n=3$, considering the diagram in fig. 11. The corresponding amplitude can be written in the general form

$$A = A_1\, A_2\, f(s_{12}, s_{23}, t_1, t_3') \,,$$

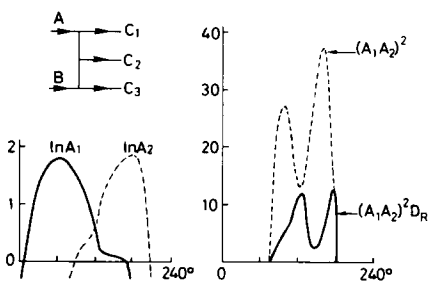

Fig. 11. Various quantities relating to a double Regge amplitude corresponding to the diagram in the upper left corner, plotted against ω for a collision $\pi N \to \pi\pi N$ at c.m. energy 10 GeV, all transverse momenta being 0.3 GeV/c. The curve for $(A_1A_2)^2\, D_R$ has an arbitrary normalization.

$$A_1 = (b + s_{12})^{\alpha_1(t_1)} , \qquad A_2 = (b + s_{23})^{\alpha_2(t'_3)} ,$$

where $\alpha_1(t_1)$, $\alpha_2(t'_3)$ are the Regge trajectories, b is a parameter $\gtrsim 1$ (we continue to use the GeV as unit), and f is a complex function remaining bounded for s_{12} and/or $s_{23} \to +\infty$. The Regge exponents and/or f ensure that A vanishes exponentially for t_1 and/or $t'_3 \to -\infty$. From figs. 9 and 10 the high-energy situation is then clear. Assuming positive slopes $d\alpha_1/dt_1$ and $d\alpha_2/dt'_3$, we find

$$0 < \omega < 120^{\circ} : A_1 \gg 1 \text{ if } \alpha_1(t_1) > 0 , \qquad A_1 \ll 1 \text{ if } \alpha_1(t_1) < 0$$

$$120^{\circ} < \omega < 180^{\circ} : A_1 \sim 1$$

$$180^{\circ} < \omega < 360^{\circ} : A_1 \ll 1$$

$$60^{\circ} < \omega < 120^{\circ} : A_2 \sim 1$$

$$120^{\circ} < \omega < 240^{\circ} : A_2 \gg 1 \text{ if } \alpha_2(t'_3) > 0 , \qquad A_2 \ll 1 \text{ if } \alpha_2(t'_3) < 0$$

$$0 < \omega < 60^{\circ} \text{ and } 240^{\circ} < \omega < 360^{\circ} : A_2 \ll 1 .$$

Fig. 11 illustrates $\ln A_1$ and $\ln A_2$ as functions of ω for

$$m_A = m_1 = m_2 = m_\pi , \qquad m_B = m_3 = m_N ,$$

$$W = 10 , \qquad \text{all } |\boldsymbol{r}_i| = 0.3 ,$$

$$\alpha_1(t) = \alpha_2(t) = \tfrac{1}{2} + t , \qquad b = 1 .$$

It also gives $(A_1A_2)^2$ and $(A_1A_2)^2 D_R$, the latter with arbitrary normalization. The peak structure obtained, which will not be qualitatively affected by the additional factor f in the amplitude, is a priori rather remarkable. Its qualitative features are readily interpreted on the basis of the general behaviour of A_1, A_2 as discussed above. Then, $(A_1A_2)^2$ has one peak for ω between 60° and 120°; it comes from the maximum of A_1 at $\omega = 60^{\circ}$ which is displaced to larger ω by A_2. The second peak of $(A_1A_2)^2$, between 120° and 180°, is produced by the maximum of A_2 at $\omega = 180^{\circ}$, displaced to smaller ω by A_1. The maxima of $(A_1A_2)^2$, however, are further displaced by the sharp peaks of D_R, i.e. of the relativistic phase-space element. These peaks occur at $\omega = 120^{\circ}$, where the pion C_2 has $q_2 = 0$, and at $\omega = 180^{\circ}$, where the pion C_1 has $q_1 = 0$. Hence, $(A_1A_2)^2 D_R$ has a peak for ω just below 120° and one for ω just below 180°. The occurrence of the latter peak is surprising because it corresponds to a situation where C_2 goes forward compared to C_1, in contradiction with the natural ordering of longitudinal momenta ($q_1 > q_2 > q_3$) expected for the diagram of fig. 11. In the region $120^{\circ} < \omega < 180^{\circ}$, A_1A_2 should show strong interference with the amplitude from the diagram obtained by interchanging C_1 and C_2.

Fig. 11 refers to a situation where all transverse momenta are 0.3. Increasing this value, one finds that the maximum of A_2 decreases faster than the one of A_1, and that the peak of $(A_1A_2)^2 D_R$ at $\omega = 180^{\circ}$ soon becomes a mere shoulder; this occurs e.g. when all $|\boldsymbol{r}_i| = 0.5$. The peak at $\omega = 120^{\circ}$, on the other hand, remains quite pronounced. Inversely, de-

creasing the $|\boldsymbol{r}_i|$ causes a more rapid increase of the $\omega = 180^{\circ}$ peak which becomes even higher than the $\omega = 120^{\circ}$ one when all $|\boldsymbol{r}_i|$ are 0.1. All these qualitative features are already present for a c.m. energy as low as 4.

These considerations clearly indicate the interest of plotting experimental data not only in longitudinal phase space, as illustrated in figs. 3 and 4, but also against the angle ω as in fig. 11. This can be done by summing over all transverse momenta or by taking characteristic intervals of them. In such plots it will be useful to give each event a weight proportional to D_{R}^{-1} so as to bring out the magnitude of the relativistically invariant matrix element. In addition, our discussion suggests that a study of transverse momentum distributions and correlations for constant ω (i.e. for ω within rather small intervals) would also be very instructive.

6. THE PRINCIPLE OF A NEW MONTE CARLO INTEGRATION METHOD

We end this paper by suggesting a new method for Monte Carlo evaluation of phase-space integrals. It is based on the separation of longitudinal and transverse momenta considered above and it is most suitable for integrals which get their main contribution from the small transverse momentum region (although it is applicable in principle to any phase-space integral). Consider the integral

$$J = \int F \, \mathrm{d}V_{\mathrm{R}}$$

where $\mathrm{d}V_{\mathrm{R}}$ is the relativistically invariant volume element considered in sect. 3, and $F(p_1, \ldots p_n)$, $p_i = (q_i, \boldsymbol{r}_i)$, is a function of the n particle momenta. The integration extends over the whole of phase space; energy conservation makes this a finite domain.

Using the definitions and results of sects. 2 and 3, we rewrite J in the form

$$J = \int F_1 \, \mathrm{d}V^{\mathrm{T}} \cdot \delta(Q)\mathrm{d}Q \cdot \delta(q - q_0)\mathrm{d}q \cdot \mathrm{d}_{n-2}\omega \, ,$$

$$F_1 = n^{-\frac{1}{2}} \, FD_{\mathrm{N}} \left(\prod_1^n E_i \right)^{-1} = n^{-\frac{1}{2}} \, FD_{\mathrm{R}} \, . \tag{13}$$

To separate the function

$$\delta_2 \left(\sum_1^n \boldsymbol{r}_i \right)$$

contained in $\mathrm{d}V^{\mathrm{T}}$, we introduce a $(n \times n)$ orthogonal O_{ij} satisfying

$$O_{in} = n^{-\frac{1}{2}} \, , \quad i = 1, \ldots n \, , \tag{14}$$

and we define new vectors $\boldsymbol{u}_1, \ldots \boldsymbol{u}_n$ through

$$\boldsymbol{r}_i = \sum_{j=1} O_{ij}\,\boldsymbol{u}_j \ . \tag{15}$$

An explicit example of such a matrix is given in the appendix. From eq. (14) and the orthogonality condition

$$\sum_{i=1}^{n} O_{ij}\,O_{ik} = \delta_{jk} \ ; \qquad j,k = 1,\ldots n \ ,$$

we conclude

$$\sum_{1}^{n} \boldsymbol{r}_i = n^{\frac{1}{2}}\,\boldsymbol{u}_n \ .$$

Furthermore, again from orthogonality,

$$\prod_{1}^{n} \mathrm{d}_2\,\boldsymbol{r}_i = \prod_{1}^{n} \mathrm{d}_2\,\boldsymbol{u}_i \ .$$

Hence

$$\mathrm{d}V^{\mathrm{T}} = n^{-1}\,\delta_2(\boldsymbol{u}_n) \prod_{1}^{n} \mathrm{d}_2\,\boldsymbol{u}_i \ .$$

Our next step is to introduce a gaussian weighing factor in the transverse momenta

$$\Phi = \exp(-\rho \sum_{1}^{n} \boldsymbol{r}_i^2) = \exp(-\rho \sum_{1}^{n} \boldsymbol{u}_i^2) \ . \tag{16}$$

Orthogonality of O_{ij} justifies equality of the two expressions. Eqs. (13) can now be written

$$J = \int F_2\ \delta(Q)\mathrm{d}\,Q \cdot \delta_2(\boldsymbol{u}_n)\mathrm{d}\,\boldsymbol{u}_n \cdot \delta(q-q_0)\mathrm{d}q \cdot (\Phi \prod_{1}^{n-1} \mathrm{d}_2\,\boldsymbol{u}_i) \cdot \mathrm{d}_{n-2}\,\omega \ ,$$

$$F_2 = n^{-\frac{3}{2}}\,F D_{\mathrm{R}}\,\Phi^{-1} \ ,$$

or, after performing the delta function integrations,

$$J = \int F_2 (\Phi \prod_{1}^{n-1} \mathrm{d}_2\,\boldsymbol{u}_i)\mathrm{d}_{n-2}\,\omega \ ,$$

where now, in Φ and F_2, the constraints

$$Q = \boldsymbol{u}_n = 0 \ , \qquad q = q_0 \ ,$$

are to be used. Note that the latter requires that condition (11) of sect. 3

holds, where the m_i' are now functions of the $\boldsymbol{u}_j$ through eq. (15). If it does not, the point $\boldsymbol{u}_1, \ldots \boldsymbol{u}_{n-1}$ contributes zero to the integral.

The proposed Monte Carlo procedure consists in generating random vectors $\boldsymbol{u}_1, \ldots \boldsymbol{u}_{n-1}$ and random polar angles $\omega_1, \ldots \omega_{n-2}$ according to the probability distribution

$$\mathrm{d}N = (\Phi \prod_1^{n-1} \mathrm{d}_2 \boldsymbol{u}_i)\mathrm{d}_{n-2}\,\omega \,,$$

$$\Phi = \exp(-\rho \sum_1^{n-1} \boldsymbol{u}_i^2) \,. \tag{17}$$

From the ω and $\boldsymbol{u}$, through eqs. (10) and (15) where the former are taken for $q = q_0$, $Q = 0$, we calculate the corresponding $q_1, \ldots q_n$, $\boldsymbol{r}_1, \ldots \boldsymbol{r}_n$ to be introduced in F_2 and we obtain for J the Monte Carlo estimate

$$J = \int F_2 \, \mathrm{d}N \,.$$

At the end of the present section we shall mention an explicit procedure to construct the polar angles $\omega_1, \ldots \omega_{n-2}$ and to calculate the functions $\gamma_i(\omega_1, \ldots \omega_{n-2})$ of eqs. (10).

For high-energy collisions, useful functions F would be such that they tend rapidly toward zero when one or more $|\boldsymbol{r}_i|$ become large, because the observed average transverse momenta are small (of order $\lesssim 0.4$ GeV). One should choose ρ such that Φ in eq. (16) has about the same range in the $|\boldsymbol{r}_i|$ as F.

In order to generate random $\boldsymbol{u}$ according to eq. (17), it seems useful to rewrite the components of $\boldsymbol{u}_i$ as

$$u_i^{(1)} = u\,\xi_{2i-1} \,, \qquad u_i^{(2)} = u\,\xi_{2i} \,, \qquad (i = 1, \ldots n-1) \,,$$

$$u = \Big(\sum_1^{n-1} \boldsymbol{u}_i^2\Big)^{\frac{1}{2}} \,, \qquad \sum_1^{2n-2} \xi_j^2 = 1 \,.$$

We have then

$$\Phi \prod_1^{n-1} \mathrm{d}_2 \boldsymbol{u}_i = u^{2n-3} \exp(-\rho u^2)\mathrm{d}u \cdot \mathrm{d}_{2n-3}\,\xi \,,$$

where $\mathrm{d}_{2n-3}\,\xi$ is the solid angle element in $(2n-2)$-dimensional space. The random distribution of u will be achieved by adopting a uniform distribution for the new variable

$$\bar{u} = \int_0^u v^{2n-3} \exp(-\rho v^2)\mathrm{d}v \,.$$

For the ξ_j, what is needed is a uniform distribution on the unit sphere of $(2n-2)$-dimensional space. A simple generation method for this distribution is given in the appendix.

We turn to the polar angles $\omega_1, \ldots \omega_{n-2}$ in the space L_{n-1}, as introduced in sect. 3. Their definition is obvious for n=3 and 4. For explicit calculations when $n > 4$, a simple procedure consists in constructing orthogonal coordinates $Q_1, \ldots Q_{n-1}$ in the space L_{n-1}, e.g. by means of the same orthogonal matrix as used above

$$q_i = \sum_{j=1}^{n-1} O_{ij}\, Q_j + n^{-\frac{1}{2}}\, Q \ .$$

We then have

$$Q_j = q\, \eta_j \ , \qquad \Sigma \eta_j^2 = 1 \ , \qquad (j = 1, \ldots n\text{-}1) \ .$$

Here, Q and q are the coordinates introduced in sect. 3, and the η_j, constrained to be on the unit sphere of $(n-1)$-dimensional space, give an explicit realization of the polar angles $\omega_1, \ldots \omega_{n-2}$. For eq. (17) we need a uniform distribution on this sphere. The construction given in the appendix can be used.

As noted before, the function D_R is strongly peaked when $q_i = 0$ for a pion. These peaks occur also in the function F_2 introduced by our Monte Carlo procedure. At very high energy it may become desirable to generate more points in the region of such peaks. This can be achieved by generating additional points on the unit sphere $\Sigma \eta_j^2 = 1$ in the region where one or more $q_i = 0$, modifying the function F_2 correspondingly.

The author is indebted to Dr. K. Zalewski for valuable suggestions concerning the Monte Carlo integration. Useful discussions with experimental and theoretical colleagues, especially Drs. A. Białas and W. Kittel, are gratefully acknowledged.

APPENDIX

A. *An explicit form for the matrix O_{ij}*

For the orthogonal matrix O_{ij}, introduced in sect. 6, the following simple choice can be made

$$O_{11} = -O_{21} = 2^{-\frac{1}{2}} \ , \qquad O_{31} \ldots = O_{n1} = 0 \ ,$$

$$O_{12} = O_{22} = -\tfrac{1}{2}\, O_{32} = 6^{-\frac{1}{2}} \ , \qquad O_{42} = \ldots = O_{n2} = 0 \ ,$$

$$O_{1,n-1} = \ldots = O_{n-1,n-1} = -(n-1)^{-1}\, O_{n,n-1} = [n(n-1)]^{-\frac{1}{2}} \ ,$$

$$O_{1n} = \ldots = O_{nn} = n^{-\frac{1}{2}} \ .$$

B. *Generation of uniform distribution on unit sphere*

We want to generate the distribution

$$dw = \delta(1 - \sum_1^N x_i^2) dx_1 \ldots dx_N , \tag{18}$$

the cases of interest being for $N \geq 4$.

For N even, $N = 2K$, we define new variables through

$$x_{2j-1} = \rho_j^{\frac{1}{2}} \cos \varphi_j , \qquad x_{2j} = \rho_j^{\frac{1}{2}} \sin \varphi_j , \qquad j = 1, \ldots K , \tag{19}$$

$$0 \leq \rho_j \leq 1 , \qquad 0 \leq \varphi_j \leq 2\pi .$$

They give

$$\sum_1^N x_i^2 = \sum_1^K \rho_j , \qquad \prod_1^N dx_i = 2^{-K} \prod_1^K d\rho_j d\varphi_j ,$$

and consequently

$$dw = 2^{-K} \delta(1 - \sum_1^K \rho_j) \prod_1^K d\rho_j d\varphi_j . \tag{20}$$

The φ_j are independent variables, uniformly distributed on $(0, 2\pi)$. To generate the ρ_j, one can take K-1 independent numbers $\sigma_1, \ldots \sigma_{K-1}$, each being uniformly distributed on the interval $(0, 1)$. For each random choice, order them according to

$$0 \leq \sigma_{j_1} \leq \sigma_{j_2} \cdots \leq \sigma_{j_{K-1}} \leq 1 ,$$

and define $\rho_1, \ldots \rho_K$ by

$$\rho_1 = \sigma_{j_1} , \qquad \rho_2 = \sigma_{j_2} - \sigma_{j_1} , \ldots \rho_K = 1 - \sigma_{j_{K-1}} .$$

The ρ so obtained obey the distribution law (20).

The treatment of eq. (18) for N odd ($N = 2K+1$) can easily be reduced to the previous one. We define ρ_j, φ_j by eq. (19) and we introduce new variables ρ_j' by

$$\rho_j = (1 - x_N^2) \rho_j' , \qquad j = 1, \ldots K .$$

The intervals are now

$$0 \leq \rho_j' \leq 1 , \qquad 0 \leq \varphi_j \leq 2\pi .$$

The distribution (18) then becomes

$$dw = 2^{-K} \delta(1 - \sum_1^K \rho_j') \left(\prod_1^K d\rho_j' \cdot d\varphi_j \right) \cdot (1 - x_N^2)^{K-1} dx_N .$$

The ρ_j', φ_j are generated as the ρ_j, φ_j were previously. For x_N, one uses a uniform distribution for the new variable

$$\bar{x} = \int_0^{x_N} (1 - x^2)^{K-1} \, dx \,, \qquad -1 \leq x_N \leq 1 \,.$$

REFERENCES

[1] L. Van Hove, Phys. Letters, to appear.
[2] Aachen-Berlin-CERN Collaboration, private communication from W. Kittel.
[3] Aachen-Berlin-Bonn-CERN-Heidelberg Collaboration, private communication from W. Kittel.
[4] Chan Hong-Mo, J. Łoskiewicz and W. W. M. Allison, Nuovo Cimento 57A (1968) 93;
O. Czyzewski, in: Proc. 14th Int. Conf. on high-energy physics (Vienna 1968), ed. by J. Prentki and J. Steinberger (CERN, Geneva 1968) p. 367, esp. § 3 p. 369.